

MHD Modeling of a Disk-Wind from a High-Mass Protobinary: the case of Orion Source I

B. Vaidya^{1*}, C. Goddi^{2,3}

¹*School of Physics and Astronomy, University of Leeds, Leeds LS29JT*

²*European Southern Observatory, Garching, Germany* ³*Joint Institute for VLBI in Europe, Postbus 2, 7990 AA Dwingeloo, The Netherlands*

10 September 2021

ABSTRACT

Very long baseline interferometry (VLBI) observations of SiO masers in Orion Source I has enabled for the first time to resolve the outflow from a high-mass protostar in the launch and collimation region. Therefore, Source I provides a unique laboratory to study mass-loss and mass-accretion in a high-mass protostar. We numerically simulate the dynamics of the disk-wind inside 100 AU from Source I. This enables us to investigate the balance of different forces (gravitational, magnetic, thermal) regulating gas dynamics in massive star formation. In this work, we adopt magnetohydrodynamic (MHD) disk-wind models to explain the observed properties of the disk-wind from Orion Source I. The central source is assumed to be a binary composed of two $10 M_{\odot}$ stars in a circular orbit with an orbital separation of 7 AU. High resolution ideal MHD wind launching simulations (which prescribe disk as a boundary) are performed using the PLUTO code. The simulations are allowed to run until a steady state is obtained. MHD driven disk-wind provides a consistent model for the wide-angle flow from Source I probed by SiO masers, reproducing the bipolar morphology, the velocity amplitude and rotational profile, the physical conditions, and the magnetic field strength.

Key words: (magnetohydrodynamics) MHD – methods: numerical – ISM: jets and outflows

1 INTRODUCTION

In the formation of low-mass stars, disks and jets play a major role in controlling mass accretion and removing excess angular momentum. Specifically, low-mass protostellar jets are expected to be launched and collimated via magneto-centrifugal processes at distances $\ll 10$ AU from Young Stellar Objects or YSOs (e. g. Konigl & Pudritz 2000). However, the balance of forces in proximity to high-mass YSOs has been difficult to infer because high extinctions, clustering, and large distances hinder attempts to resolve the gas structure and dynamics at small radii (< 100 AU) where outflows are launched and collimated from accretion disks.

Radio source I in Orion BN/KL is the nearest example of a high-mass YSO. The close distance and exceptional richness in molecular maser tracers enabled the best detailed picture of gas dynamics in a massive YSO on scales comparable with the Solar System. In particular, detailed imaging of vibrationally-excited states SiO masers with the Very Long Baseline Array (VLBA) enabled resolving the surface of an edge-on disk as well as a wide-angle outflow in the collimation and launch region at radii 10-100 AU (Matthews et al.

2010; Figure 1). Additionally, at larger radii (100-1000 AU), the wide-angle wind appears to collimate in a straight bipolar flow, as traced by H₂O and $\nu=0$ SiO maser and thermal emission (Plambeck et al. 2009; Greenhill et al. 2012). Measurement of the 3D velocity fields of SiO masers provides a clear evidence of rotation in both the disk and the wind along the same axis. Cunningham et al. (2005). explored the importance of stellar winds from a luminous central source and proposed the idea that SiO masers in Source I may arise from the interaction of a spherical wind with an infalling envelope. However, Matthews et al. (2010) argued that such a model could not explain in detail the gas dynamics and physical conditions as revealed by SiO masers and alternately proposed that the SiO masers arise from material ablated from the surface of an accretion disk and discussed qualitatively the applicability of various classes of disk-wind models to Source I. They find evidence to support that magnetic fields may play a role in driving and/or shaping the disk-wind from Source I, based on details of gas dynamics on small scales, like curved and helical trajectories traced by maser motions. Assuming a magnetic field is present, a magneto-centrifugally launched wind (e.g., Blandford & Payne 1982; Konigl & Pudritz 2000; Fendt 2006) would be a natural candidate for powering a disk-wind from

* E-mail: B.Vaidya@leeds.ac.uk (BV)

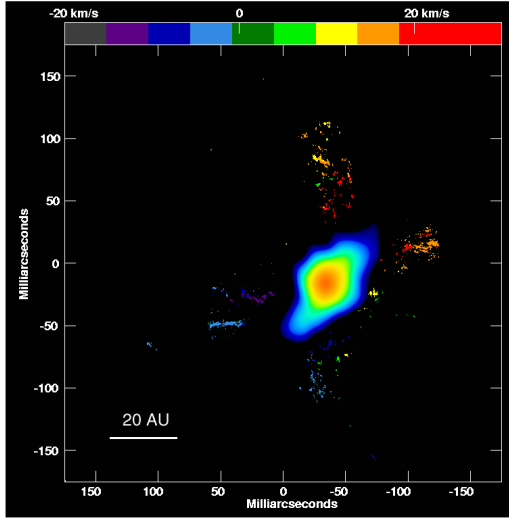


Figure 1. Velocity field (in km/s) of the SiO $v=1,2$ $J=1-0$ maser emission in Orion Source I as observed with the VLBA (Matthews et al. 2010). The stellar velocity is ~ 6 km s $^{-1}$. The bulk of the SiO emission is located within four “arms” of an X-shaped pattern, while a ~ 14 AU thick band with no SiO emission harbors the 7mm continuum source (Reid et al. 2007; Goddi et al. 2011). The continuum emission traces an ionized disk while the SiO masers probe material ablated from the surface of the disk in a wind.

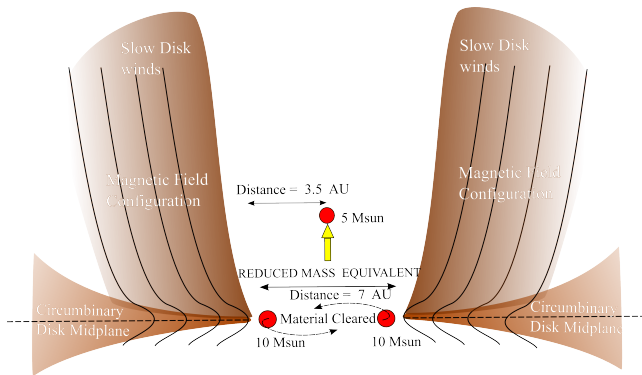


Figure 2. Cartoon Model for Source I.

Source I. The latter thus becomes an ideal laboratory to extend the MHD models from solar-like stars to massive YSOs. Recently, Vaidya et al. (2011) explored the interplay of radiation forces and magnetic fields to show that radiative line driving from luminous stars with masses $> 30 M_{\odot}$ does modify the dynamics of outflows. However, since the luminosity for a $10 M_{\odot}$ binary Orion Source I would be less than a single $20 M_{\odot}$, we adopt that model in the ideal MHD regime (neglecting radiative force) to numerically simulate the dynamics of the disk-wind inside 100 AU.

2 MODEL ASSUMPTIONS

The initial conditions adopted to model the disk-wind from Orion Source I are reported in Table 1 and are derived from either observations and/or modeling of the system. Source I is believed to be an eccentric, hard binary with a total mass of $2 \times 10 M_{\odot}$, based on studies of the dynamics of

YSOs and molecular gas in Orion BN/KL, as well as N-body simulations (Goddi et al. 2011; Bally et al. 2011). In particular, proper motion measurements of radio sources provided strong evidence that a dynamical interaction occurred about 500 years ago between massive YSOs Source I and BN (e. g., Goddi et al. 2011). N-body numerical simulations showed that the dynamical interaction between a binary of two $10 M_{\odot}$ stars (Source I) and a single $10 M_{\odot}$ star (BN) may lead to simultaneous ejection of both stars and the BN/KL outflow as well as binary hardening, while preserving the original circumbinary disk around Source I (Bally et al. 2011; Moeckel & Goddi 2012). Mechanical energy conservation (and virial theorem) implies an orbit semi-major axis $a_0 = 2 - 5$ AU, depending on the estimate of the kinetic energy of the runaway stars and the molecular gas flow (Goddi et al. 2011; Bally et al. 2011). For simplicity, we neglect the eccentricity and assume that the system is an equal-mass circular binary, comprised of two $10 M_{\odot}$ stars orbiting in a circle of radius $a_0 = 3.5$ AU.

A high-resolution study of H α and [O I] $\lambda 6300$ line profiles in a pre-main-sequence spectroscopic binary has shown evidence of a bipolar jet as being launched by the whole binary as opposed to each star individually (Mundt et al. 2010). Similarly, we assume that the binary members orbit inside the inner radius of a truncated circumbinary disk and that the wind is launched at this radius. The cartoon figure representing our model assumption is shown in Fig. 2.

To study the wind launching from Source I, we perform axi-symmetric ideal MHD simulations in cylindrical coordinates (r, ϕ, z) using the PLUTO code (Mignone et al. 2007). We essentially prescribe a hydrostatic corona (density and pressure) threaded with force-free magnetic field. An adiabatic equation of state, $P = \frac{\gamma-1}{\gamma} \rho^\gamma$, with $\gamma = 5/3$, relates the pressure with the density in the flow. For the central gravity, we treat the system of equal mass binary members as an equivalent $5 M_{\odot}$ (reduced mass) object at their barycenter. The accretion disk which is treated as a boundary forms the launching base of the wind (e.g., Ouyed & Pudritz 1997). Further, we choose the wind launching point to be at a distance equal to the radius of the binary orbit, i.e. $r_0 = a_0$, where the material is rotating with a sub-Keplerian velocity $V_\phi = \chi v_0$. Further, the disk is considered to be denser than the hydrostatic corona and this density contrast is prescribed by δ . In a realistic (thick and hot) disk, the central gravity is balanced radially by contributions from thermal pressure and centrifugal rotation. This can be ensured by consistently deriving the sub-Keplerianity(χ) based on the choice of density contrast. For example, smaller values of δ implies a hotter (denser) disk and a larger contribution of thermal pressure resulting in the disk to rotate with sub-Keplerian speeds to maintain radial balance. We chose $\delta \sim 3$ as a reference value implying the underlying disk to rotate at a speed 0.8 times the Keplerian speed.

The magnetic field strength is prescribed by the value of plasma beta (the ratio of thermal pressure to the magnetic pressure) at r_0 , β_0 . In order to put constraints on the magnetic field strengths in Source I, we study the wind properties with varying β_0 (see Sect. 3.3). Finally, we assume the number density at r_0 to be $n_0 = 3 \times 10^{10} \text{ cm}^{-3}$. Reid et al. (2007) argued the disk in Source I to be ionized with a typical electron density of $\sim 10^7 \text{ cm}^{-3}$ (their “Model C”), which corresponds to an ionization fraction of $\sim 10^{-3}$.

Table 1. Parameters chosen for the reference run to study MHD driven outflow from Orion Source I.

Quantity	Reference Value
Masses of Binary [m_1, m_2]	$10 M_\odot, 10 M_\odot$
Orbital Separation [$2a_0$]	7 AU
Reduced Stellar Mass [μ_*]	$5 M_\odot$
Wind Launching radius [r_0]	3.5 AU
Keplerian Velocity at r_0 [v_0]	35.7 km s^{-1}
Volume Density at r_0 [ρ_0]	$5.0 \times 10^{-14} \text{ g cm}^{-3}$
Plasma Beta at r_0 [β_0]	1.0
Density Contrast [δ]	2.85

The flow is freely allowed to leave the outer boundaries ($r, z = 50 a_0, 150 a_0$) and symmetric boundary conditions are applied on the $r=0$ axis. The poloidal component of the magnetic field at the outer boundaries is set to avoid artificial collimation by ensuring zero current ($\nabla \times \vec{B} = 0$; Ustyugova et al. 1999; Porth & Fendt 2010). The critical boundary at $z=0$ mimics the inflow of gas and magnetic flux from the disk surface. Here, we ensure the disk to be in pressure equilibrium with the medium but with a higher density (i.e. colder than the medium). The angular speed of the magnetic field line in the disk is equal to the Keplerian value and the poloidal velocity is updated each time with the value at the grid cell just above the boundary. Further, ideal MHD approximation permits to set the flow velocity along the poloidal magnetic field ($v_p \parallel B_p$). Thus, the mass flux at the disk boundary is not fixed but consistently derived by causal interaction between the outflowing gas and the boundary value. Detailed description of these boundary conditions are given in Vaidya et al. (2011).

3 RESULTS AND DISCUSSION

3.1 MHD driven wind profiles

At the onset of our reference run, material at the base of the disk is ejected in vertical direction along the magnetic field. This material propagates outwards producing bow shocks in the ambient medium. As this shock propagates outside of the domain, the flow collimates due to magnetic forces until a steady equilibrium is attained, beyond which no further evolution of magnetic field lines takes place. The steady-state values of the density, poloidal and azimuthal velocities of the wind are shown in Figure 3, along with the magnetic field lines (in red), the poloidal velocity versors (white arrows), temperature contours and MHD critical surfaces. The magnetic field lines ideally mark the morphology of the outflow. The left panel of Figure 3 shows the steady-state number density of the fluid, whose values range from 10^8 cm^{-3} to 10^{11} cm^{-3} . Overlaid on the density map are the temperature contours, with values ranging from 5000 K closer to the central source to 100 K at large distances. The high density and temperatures close to the axis reflect the fact that the initial hydrostatic conditions are fixed at the boundary inside of the wind launching radius (this ensures numeri-

cal stability of the flow very close to the axis). The middle panel of Figure 3 shows the poloidal wind velocity, whose values range from 8.0 to 32.0 km s^{-1} . The lines over-plotted show three critical surfaces in a steady-state MHD flow, viz. the magneto-sonic surface (yellow), the magneto-fast surface (black), and the Alfvén surface (red). The flow starts sub-magneto-sonically from the disk and is accelerated to super fast speeds mainly via Lorentz forces. The Alfvén surface marks the locus of points in the flow where ideally the kinetic energy of the flow is converted to magnetic energy. This results in bending of the field lines thereby generating a toroidal field and corresponding hoop stress which collimates the flow. The right panel of Figure 3 finally shows the azimuthal component of the wind velocity, with values ranging from 10 km s^{-1} at the outer edge to 25 km s^{-1} close to the inner wind launching point. The transfer of angular momentum from the wind to the medium may impart rotation to the latter, as observed in SiO masers (Sec. 3.2).

3.2 Comparison between MHD wind models and wind properties observed from SiO masers

We propose that the SiO masers in Orion Source I are excited as a moderately rotating disk-wind interacts with the ambient medium via slow MHD shocks and transfer of angular momentum. Similar mechanisms have been successfully applied to explain the excitation of H₂O masers (Kaufman & Neufeld 1996). Here, we qualitatively compare the steady-state properties of a single-fluid, rotating MHD wind (launched from an underlying accretion disk) with the observed physical and dynamical properties of the outflow molecular component probed by SiO masers in Source I.

Three physical properties of the wind from the MHD modeling are consistent with SiO maser observations: temperature/density profiles, morphology, and velocity field.

The conditions for optimum excitation of the SiO maser emission are $n(\text{H}_2) \sim 10^9 \text{ cm}^{-3}$ and $T \lesssim 2000 \text{ K}$, respectively, as derived from a radiative transfer analysis by Goddi et al. (2009). In our simulations, the regions close to the inner launching point ($z, r \lesssim 15 \text{ AU}$) have values of densities ($10^{10-11} \text{ cm}^{-3}$) and temperatures (2000-5000 K) beyond the critical values required for SiO maser excitation (Fig. 3, left panel). This is consistent with the 14 AU thick "dark band" seen in Fig. 1 where no masers are observed. The intermediate region ($15 \text{ AU} < z, r < 60 \text{ AU}$) has typical densities of 10^9 cm^{-3} and $T \sim 1000 - 2000 \text{ K}$ (Fig. 3, left panel). Here, the wind can provide a strong IR background source for pumping the SiO masers in the shocks produced by its interaction with the ambient molecular medium.

In the steady-state, the magnetic collimation and acceleration result in an open funnel shaped structure of field lines (Fig. 3). Such a configuration of magnetic flux surfaces naturally results in a disk-wind with wide-angle bipolar morphology, which resembles the X-shaped wind structure around Source I revealed by SiO maser emission (Fig. 1).

Regarding the velocity field, the dynamical properties of molecular outflows can be extrapolated from the single-fluid MHD wind by analyzing the momentum transfer (Masson & Chernin 1993). In this study, the density of the MHD driven wind exceeds the mean density of its surrounding medium. Such dense and cold winds carry a large amount of momentum and impart a significant fraction of it to the ambient

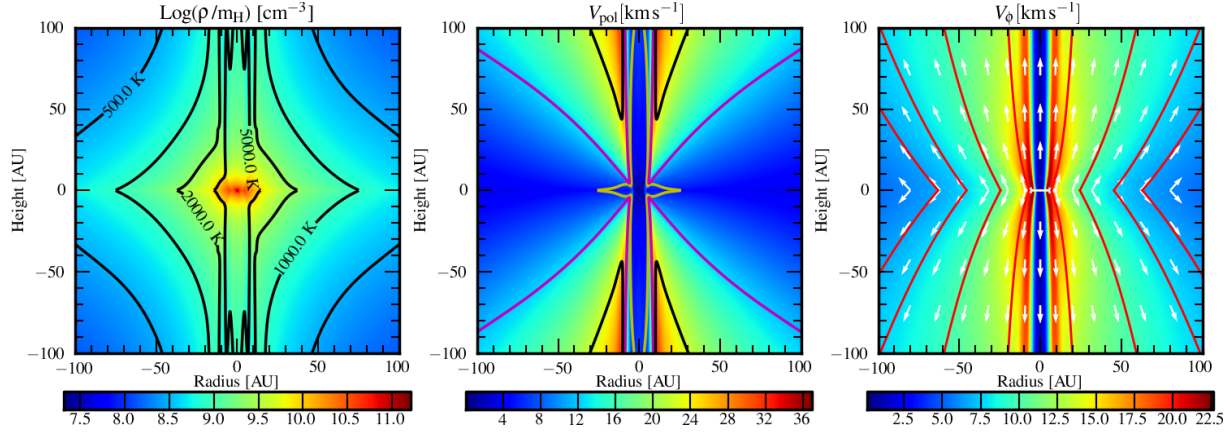


Figure 3. Number density (left), poloidal velocity (middle) and azimuthal velocity (right) of the reference run in steady-state. Temperature contours (black) for $T = 500$ K, 1000 K, 2000 K and 5000 K are overlaid in the left panel. The middle panel shows the positions of three MHD critical surfaces - magneto-sonic surface (yellow), Alfvén surface (magenta), magneto-fast surface (black). White arrows in the right panel represents the velocity vectors which are parallel to magnetic field lines shown by solid red lines.

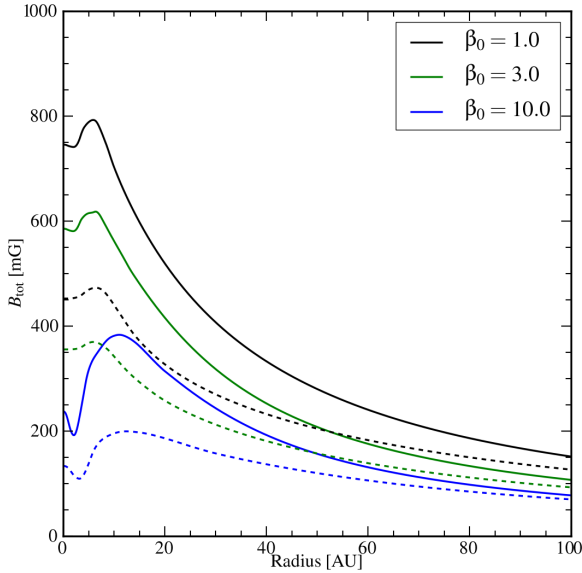


Figure 4. Radial profiles of the magnetic field [in mG] at $z = 20$ AU [solid] and $z = 60$ AU [dashed] for the reference run, obtained after the MHD wind has reached a steady-state.

medium, resulting in the shocked material to have velocities of the same order as the wind itself (Masson & Chernin 1993), i.e. in the range of $10 - 30 \text{ km s}^{-1}$ (Fig. 3, middle panel). Consistently, Matthews et al. (2010) measured the 3D velocities of the molecular gas flows around Source I, to vary in the range from 5 km s^{-1} to 25 km s^{-1} , with an average of 14 km s^{-1} . In addition, SiO masers show rotation seen as a velocity gradient in the radial velocities of the four arms of the "X" tracing the disk-wind, which is consistent with the trend obtained for V_ϕ (Figure 3, right panel).

Therefore, the simulated MHD winds can drive molecular flows by interacting via shocks with the ambient medium.

3.3 Magnetic field strength

In our models, the magnetic field strength is governed by β_0 . We have carried out simulation runs with three differ-

ent values of β_0 viz. 1.0, 3.0 and 10.0. Figure 4 shows the radial profiles of magnetic field strength at $z = 20$ AU and $z = 60$ AU for different values of β_0 and $\delta = 2.85$. We find that the magnetic field strength varies in the range $0.2 - 0.8$ G (depending on β_0) and decreases with radius and/or vertical height. From this study, we observe that the changes in density and temperature are not significant with varying β_0 (e.g., $\Delta T \sim 100 - 200 \text{ K}$ when β_0 increases by ten fold). On the other hand, poloidal and azimuthal velocities decrease substantially with increasing values of β_0 . Since lower field strengths imply lower Lorentz force, the flow is not efficiently accelerated resulting in lower velocities. The typical velocities obtained from $\beta_0 > 3.0$ are not enough to explain the observed velocities in Source I. Therefore, we assume as a reference the magnetic field strength corresponding to $\beta_0 = 1$, ~ 0.35 G (at $r, z = 40 \text{ AU}, 20 \text{ AU}$). Assuming equipartition, Matthews et al. (2010) quote a magnetic field strength of ~ 0.3 G for Source I, based on kinematics of SiO masers. This value is consistent with a measurement of OH 1665 MHz masers across a $\sim 10^4$ AU region around Source I, which provided field strengths of 1.8 to 16.3 mG (Cohen et al. 2006). Since the OH masers are believed to arise from material with $n(\text{H}_2) \sim 10^7 \text{ cm}^{-3}$ (Gray et al. 1992) and the magnetic field strength is expected to scale as the square root of the gas density, a simple extrapolation from the large scales (probed by OH masers) to the small scales (probed by SiO masers) gives field strengths of order the value predicted by the equipartition assumption. These empirical estimates lie comfortably within the range predicted by our model, but direct measurements via the Zeeman effect could provide a more reliable comparison between models and observations.

3.4 Model Limitations

The main qualitative features of a steady MHD driven disk-wind are consistent with the physical and dynamical properties of the molecular flow probed by SiO masers. A more quantitative analysis requires however further theoretical and observational studies. In this section, we list the limitations of the present model and the scope for future work.

- (i) The assumption of treating the disk as a bound-

ary allows us to follow wind dynamics till a steady state is reached, but neglects the impact of disk dynamics on wind propagation. A more realistic model should allow both disk and outflow to evolve simultaneously (e.g., Casse & Kepkens 2002; Sheikheezami et al. 2012). Also, we neglect any feedback on the disk-wind from a stellar wind (Source I has however a rather modest $L_{\text{bol}} \sim 10^4 L_{\odot}$; Gezari et al. 1998).

(ii) In our ideal MHD model, we have assumed a single fluid MHD driven wind and have ignored effects due to diffusion of neutral molecules across the magnetic field. Though the regions close to the star are hot and potentially have a high degree of ionization, consistent with an ideal approximation, a more accurate model should incorporate effects due to diffusion between the neutral and ionized medium. Future simulations will relax the ideal MHD approximation and explore effects of magnetic diffusivity.

(iii) We have ignored any feedback due to molecular chemistry. Ideally, a direct comparison between MHD models and maser observations would require a detailed multi-fluid chemical model. Recently, conditions for molecular survival in MHD disk-winds were computed using chemical evolution of a self-similar MHD wind model (Panoglou et al. 2012). However, such a chemical model with micro-physics of maser excitation is quite complex. As a follow-up, we plan to include non-equilibrium cooling and separately follow the evolution of neutral and ionized gas fraction in the flow.

(iv) Including in the modeling the elements discussed above, requires measurement of relevant physical quantities within the launching region ($\lesssim 100$ AU), i.e. ionization degree, molecular abundances, and magnetic field strengths. High resolution and sensitive observations of Hydrogen radio recombination lines (with JVLA and ALMA) will help us constrain the dynamical and physical properties of ionized gas. Further, radiative transfer analysis of rotational molecular lines (from ALMA) can constrain molecular gas properties and abundances. Finally, polarimetric observations of SiO masers (with VLBI) will enable to measure magnetic field strength and orientation at the disk/jet interface.

4 SUMMARY

We have explored the plausibility of MHD driven wind model to explain the disk-wind properties in Orion Source I as probed by SiO masers. In particular, we have performed axisymmetric MHD wind launching simulations treating Source I as an equal mass binary and choosing initial parameters derived from observations. We propose that the SiO masers are excited as the MHD driven wind interacts with the ambient molecular medium in form of shocks. Four elements of consistency support this hypothesis:

- (i) Our model consistently reproduces the bipolar morphology of the disk-wind traced by the SiO masers.
- (ii) The poloidal and azimuthal velocities from the simulations are in the range of $10 - 30 \text{ km s}^{-1}$, which agree very well with the observed average 3D velocity of 14 km s^{-1} and with the rotational component of SiO masers.
- (iii) The physical conditions in the modeled wind are consistent with the requirements for pumping SiO masers.
- (iv) We predict field strengths of $0.2\text{-}0.8 \text{ G}$ within 100 AU , in agreement with empirical estimates from SiO masers.

We conclude that the main dynamical features of the SiO masers disk-wind in Orion Source I can be explained by the MHD wind model. In a broader context, Source I has provided a unique laboratory to extend the standard MHD models from low-mass to high-mass YSOs, indicating that in both regimes similar physics may describe the transfer of matter and angular momentum between disks and outflows.

ACKNOWLEDGMENTS

We thank Christian Fendt and Lynn Matthews for their valuable comments. B.V thanks the STFC for funding.

REFERENCES

- Bally J., Cunningham N. J., Moeckel N., Burton M. G., Smith N., Frank A., Nordlund A., 2011, *ApJ*, 727, 113
- Blandford R. D., Payne D. G., 1982, *MNRAS*, 199, 883
- Casse F., Kepkens R., 2002, *ApJ*, 581, 988
- Cohen R. J., Gasiprong N., Meaburn J., Graham M. F., 2006, *MNRAS*, 367, 541
- Cunningham A., Frank A., Hartmann L., 2005, *ApJ*, 631, 1010
- Fendt C., 2006, *ApJ*, 651, 272
- Gezari D. Y., Backman D. E., Werner M. W., 1998, *ApJ*, 509, 283
- Goddi C., Greenhill L. J., Chandler C. J., Humphreys E. M. L., Matthews L. D., et. al. 2009, *ApJ*, 698, 1165
- Goddi C., Humphreys E. M. L., Greenhill L. J., Chandler C. J., Matthews L. D., 2011, *ApJ*, 728, 15
- Gray M. D., Field D., Doel R. C., 1992, *A&A*, 262, 555
- Greenhill L. J., Goddi C., Chandler C. J., Humphreys E. M. L., Matthews L. D., 2012, in *IAU Symposium* Vol. 287, . pp 166–170
- Kaufman M. J., Neufeld D. A., 1996, *ApJ*, 456, 250
- Konigl A., Pudritz R. E., 2000, *Protostars and Planets IV*, p. 759
- Masson C. R., Chernin L. M., 1993, *ApJ*, 414, 230
- Matthews L. D., Greenhill L. J., Goddi C., Chandler C. J., Humphreys E. M. L., Kunz M. W., 2010, *ApJ*, 708, 80
- Mignone A., Bodo G., Massaglia S., Matsakos T., Tesileanu O., Zanni C., Ferrari A., 2007, *ApJS*, 170, 228
- Moeckel N., Goddi C., 2012, *MNRAS*, 419, 1390
- Mundt R., Hamilton C. M., Herbst W., Johns-Krull C. M., Winn J. N., 2010, *ApJ*, 708, L5
- Ouyed R., Pudritz R. E., 1997, *ApJ*, 482, 712
- Panoglou D., Cabrit S., Pineau Des Forêts G., Garcia P. J. V., Ferreira J., Casse F., 2012, *A&A*, 538, A2
- Plambeck R. L., Wright M. C. H., Friedel D. N., Widicus Weaver S. L., Bolatto A. D., Pound M. W., Woody D. P., Lamb J. W., Scott S. L., 2009, *ApJ*, 704, L25
- Porth O., Fendt C., 2010, *ApJ*, 709, 1100
- Reid M. J., Menten K. M., Greenhill L. J., Chandler C. J., 2007, *ApJ*, 664, 950
- Sheikheezami S., Fendt C., Porth O., Vaidya B., Ghanbari J., 2012, *ApJ*, 757, 65
- Ustyugova G. V., Koldoba A. V., Romanova M. M., Chechetkin V. M., Lovelace R. V. E., 1999, *ApJ*, 516, 221
- Vaidya B., Fendt C., Beuther H., et. al. 2011, *ApJ*, 742, 56